Journal of Visualization, Vol. 4, No. 2 (2001) 169-178

Flow Field Measurements of Leading-edge Separation Vortex Formed on a Delta Wing with Vortex Flaps

Rinoie, K.*

* Department of Aeronautics and Astronautics, The University of Tokyo, Hongo, Tokyo 113-8656, Japan.

Received 8 November 2000.
Revised 10 February 2001.

***Abstract*:** Wind tunnel tests are carried out using a 70° delta wing model with leading-edge vortex flaps. The structure of the leading-edge separation vortex over the leading-edge vortex flap is measured by use of a 5 holes pitot probe, surface pressure measurement technique and oil flow visualization technique. Separation vortices formed on a plain delta wing, on a vortex flap and inboard the vortex flap hinge line are clearly visualized. Results indicate that the flow around the vortex flaps is classified into several different cross flow patterns. The streamwise flap deflection angle is defined to discuss the vortex flap performance. The optimum lift to drag ratio is attained when the amount of the wing angle of attack is not far different from that of the streamwise flap deflection angle, as long as the vortex flap is deflected modestly.

***Keywords*:** vortex flap, leading-edge separation vortex, delta wing, cross flow pattern, aircraft performance.

1. Introduction

The leading-edge vortex flap (LEVF) is one of the devices that can improve the aerodynamic efficiency of delta wings at low speeds (Rao, 1979). The LEVF is a full span deflectable flap attached to the leading-edge of the delta wing. With the flap deflected downward, a leading-edge separation vortex is formed over the forward facing flap surface (Fig. 1). The suction force generated by the vortex acts on the flap surface and generates a thrust component. Hence it reduces the drag and improves the lift/drag ratio (L/D), an essential factor for the improvement of the take-off and climb performance of the delta wing aircraft, one of the next generation supersonic civil transport aircrafts (SST). Many tests have been made which confirm the benefit of the LEVF (Campbell and Osborn, 1986). The author has made experimental studies using delta wing models that have sweepback angles Λ of 50°, 60° and 70°, fitted with tapered vortex flaps (Rinoie and Stollery, 1994; Rinoie et al., 1997; Rinoie, 1997). Purposes of these studies were to confirm the benefit of the LEVF and to know how the difference of the sweepback angle affects the aerodynamic characteristics of the wing with the LEVF.

Throughout these studies, it was revealed that the highest lift/drag ratio for the 60° delta wing is achieved using a modest LEVF deflection angle that causes the flow to attach on the flap surface without any large separation (Rinoie and Stollery, 1994). On the contrary, the maximum lift/drag ratio for the 70° delta wing is attained, when a separated region is formed on the vortex flap and when the spanwise length of this separated region almost coincides with the vortex flap width (Rinoie et al., 1997). The latter results agreed with the observations obtained for the 74° delta wing by Rao (1979). These results suggest that the formation and the behavior of the leading-edge separation vortex over the LEVF surface should be investigated more in detail, in order to get the maximum understandings of the performance of the LEVF. In this paper, both the behaviors of the leading-edge separation vortex formed on the LEVF and the effect of the LEVF over the delta wing performance

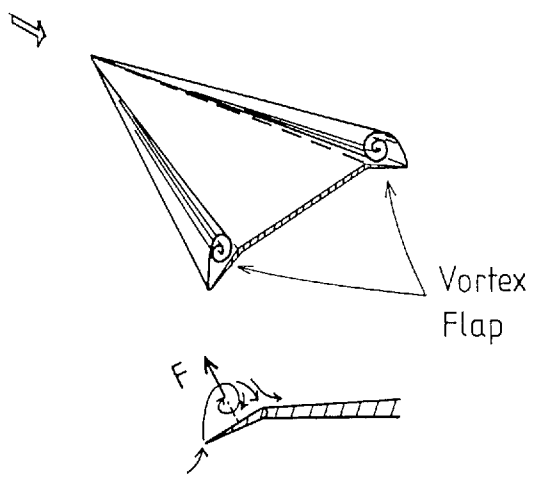

Fig. 1. Concept of vortex flap (Rinoie and Stollery, 1994).

are discussed using the results of surface pressure measurements, surface flow visualization and 5 holes pitot probe measurements for the 70° delta wing with the LEVF that was tested in Rinoie et al. (1997).

2. Experimental Details

Experimental details are summarized in this section. Figure 2 (Rinoie et al., 1997) shows details of the delta wing model of $\Lambda = 70^{\circ}$. The model is a 70° flat plate delta wing with no camber and with sharp leading-edges. The centerline chord length C is 0.5m and the thickness is 0.015m. The model has the LEVF hinge lines running from

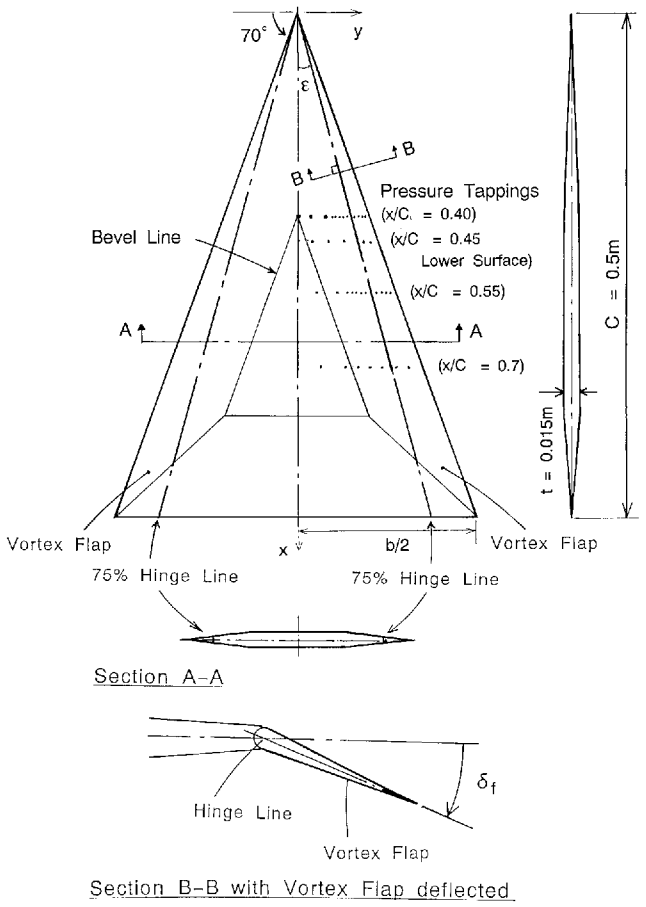

Fig. 2. 70° Delta wing model with LEVF (Rinoie et al., 1997).

the wing apex to 75% of the trailing-edge semi-span station. Three rows of pressure tapping were located on the upper surface and one row on the lower surface. The flap deflection angle δ_f is defined as the angle measured in the plane normal to the hinge line. Flap can be deflected from $\delta_f = 0^\circ$ to 50°, with an increment of 10°.

The experiments were made in a 2 m × 2 m low speed, closed working section, closed return wind tunnel at the National Aerospace Laboratory in Japan. All tests were done at a tunnel speed of $U_\infty = 30$ m/s. The Reynolds number based on the wing centerline chord Re_C was 1×10^6. The incidence range covered was from -10° to $+40^\circ$. Lift, drag and pitching moments were measured using a six-component pyramidal-type balance. Surface pressure measurements were made using Electronic Scanner Pressure Sensors (ESP). Surface oil flow and surface tuft visualizations have been conducted. Flowfield measurements have also been carried out using a 5 holes pitot probe of 1.8 mm diameter. The probe was traversed in planes perpendicular to the freestream direction using the tunnel traversing gear system. The three component velocities and total pressure coefficient were analyzed using the measured data. Because of the restriction of 5 holes pitot probe, the velocity vector which is declined more than 30° from the free stream direction or which is slower than 10 m/s could not be evaluated. The blockage effect of the 5 holes pitot probe over the model has been checked by measuring the forces and surface pressure distributions, when the probe is traversed near the model surface. The results indicated that the effect of the probe is negligible if the angle of attack of the model is less than 25°.

Unsteady flow behavior may exist when the flap deflection angle or the wing angle of attack is large. However, since the results of the 5 holes pitot probe represent only the mean flow, this unsteadiness could not be evaluated in this test. Furthermore, the leading-edge separation flow strongly depends on the flow nature on the upper surface of the wing. Hummel (1978) tested a 76° sharp delta wing model at $Re_C = 0.9 \times 10^6$. The laminar flow was observed on the upper surface. Present experiments were conducted at similar Reynolds number. It can be deduced that the flow on the upper surface is laminar at the present experiments. However, more detailed measurements are necessary to investigate the influence of the flow nature.

3. Experimental Results

Figure 3 shows the $L/D - C_L$ distributions for the wing with and without flap deflection for the 70° delta wings at $\delta_f = 0^\circ$, 20°, 30° and 50° measured by Rinoie et al. (1997). Improvements of L/D for $\delta_f = 20^\circ$ and 30° as compared with that for $\delta_f = 0^\circ$ are observed in this figure. This clearly indicates the benefit of the vortex flaps. The $\delta_f = 50^\circ$ wing does not indicate any benefit on L/D.

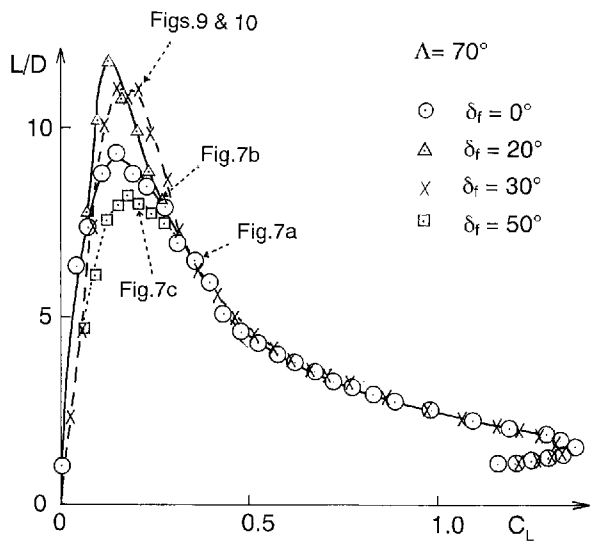

Fig. 3. Effect of LEVF on L/D vs. C_L.

Figure 4 shows an example of oil flow and surface tuft visualizations for $\delta_f = 0^\circ$ at $\alpha = 12^\circ$. Oil flow visualization was made on the left wing. Tufts were attached on some part of the right wing surface to supplement the oil flow visualization. Oil flow patterns and movements of the tufts clearly indicate the existence of a pair of leading-edge vortices on the wing. Figure 5 shows the surface flow patterns sketched from oil flow pictures at $\alpha = 9^\circ$

for different flap deflection angles d_f. The patterns define the vortex positions on the wing and flap surfaces. In this figure, H.L. denotes the vortex flap hinge line. The leading-edge separation vortex is clearly recognized for d_f = 0° and 30° (Figs. 5(a) and 5(b). Figure 5(c) shows that vortices are formed inboard the flap hinge line and on the

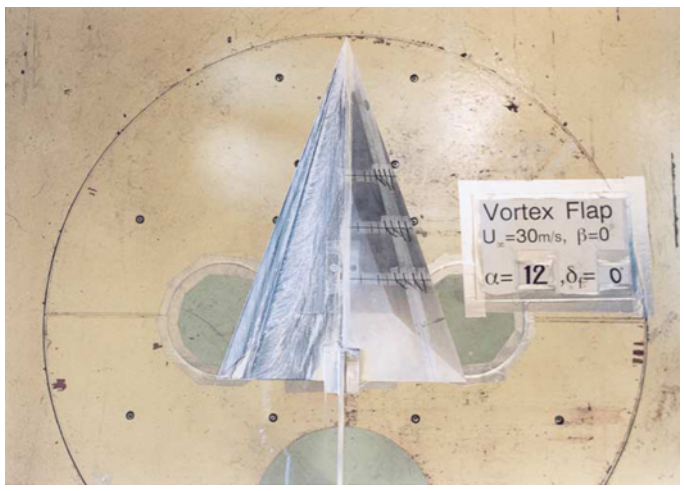

Fig. 4. Oil flow and tuft visualizations for d_f = 0° at a = 12°.

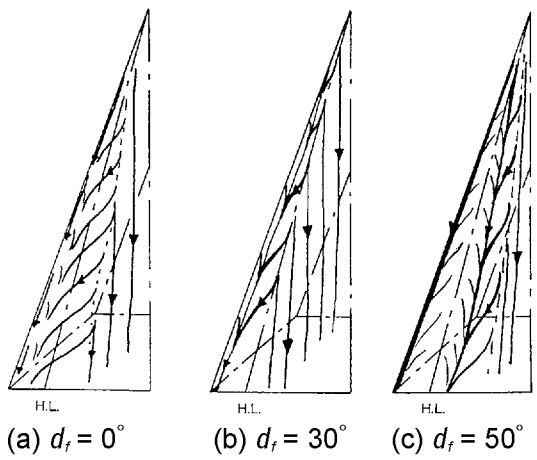

Fig. 5. Surface flow patterns at a = 9°.

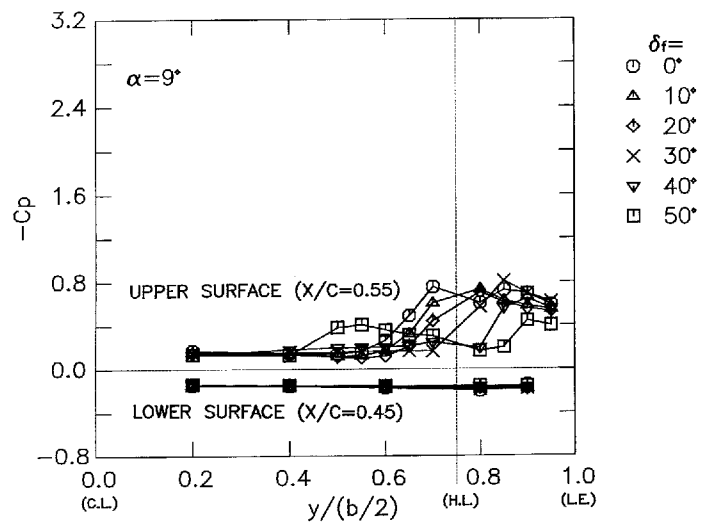

Fig. 6. Surface Pressure Distributions at a = 9°, x/C = 0.55.

flap surface for the wing with $d_f = 50^\circ$.

Figure 6 shows the surface pressure distributions for the upper surface at $x/C = 0.55$ and for the lower surface at $x/C = 0.45$ when $a = 9^\circ$, plotted against the semi-spanwise station $y/(b/2)$. Results of $d_f = 0^\circ$, 10°, 20°, 30°, 40° and 50° are shown. Suction regions are seen for all measured flap deflection angles of d_f, e.g. at $y/(b/2) = 0.6 \sim 1.0$ for $d_f = 0^\circ$, at $y/(b/2) = 0.65 \sim 1.0$ for $d_f = 20^\circ$ and at $y/(b/2) = 0.7 \sim 1.0$ for $d_f = 30^\circ$. The suction region is thought to correspond to the leading-edge separation vortex. The spanwise length of the suction region for $d_f = 30^\circ$ is shorter than that for $d_f = 0^\circ$ and almost coincides with the vortex flap spanwise length. For $d_f = 50^\circ$, the suction region is also seen inboard the flap hinge line ($y/(b/2) = 0.4 \sim 0.75$). This suggests that a separation region is formed inboard the hinge line. These results agree with the oil flow observation in Fig. 5. The lower surface pressure distributions

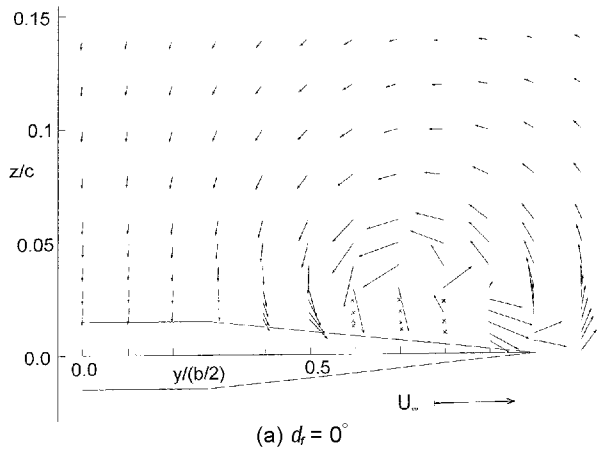

(a) $d_f = 0^\circ$

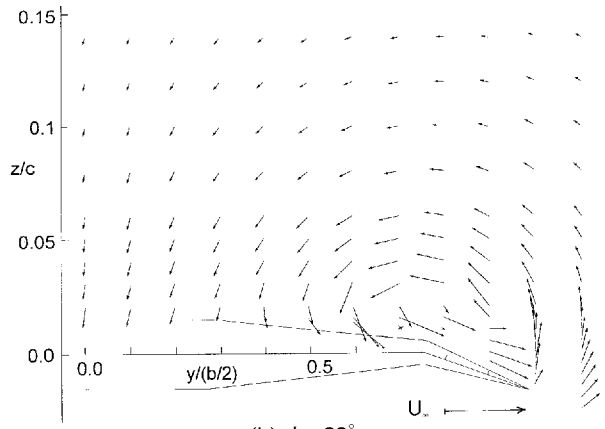

(b) $d_f = 20^\circ$

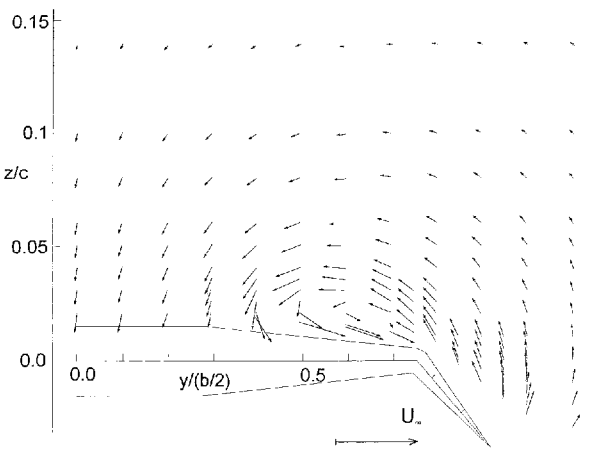

(c) $d_f = 50^\circ$

Fig. 7. Velocity vector components in the cross flow plane at $a = 9^\circ$, $x/C = 0.55$.

show very little change with d_f.

Figure 7 shows the vectors of the velocity component in the plane perpendicular to the freestream direction for the same cases as in Fig. 6 ($d_f = 0^\circ$, 20° and 50° at $a = 9^\circ$), measured by the 5 holes pitot probe. The measured amounts of L/D for each configuration are shown in Fig. 3. For $d_f = 0^\circ$ (Fig. 7(a)), it is clearly seen that the leading-edge separation vortex is formed on the wing. The $\times$ sign in this figure denotes that the magnitude or the direction of velocity vector has exceeded the measurement accuracy as was denoted in the experimental apparatus section. It is known that a secondary separation vortex is formed inside the leading-edge separation vortex on a delta wing. However, the secondary separation region inside the vortex could not be measured clearly in this tests, because of the limited number of measurement points by the 5 holes pitot probe.

Fig. 7(b) shows the velocity vector distributions for $d_f = 20^\circ$. It is seen that the separation occurs at the leading-edge and the separation vortex is formed and extends toward about $y/(b/2) = 0.5$. Fast outward flows are observed on the upper surface near the leading-edges both for Figs. 7(a) and 7(b). It is thought that the occurrence of secondary separation inside the leading-edge separation vortex causes the fast outward flow. Figure 7(c) shows the results for $d_f = 50^\circ$. Because of a large flap deflection angle, the 5 holes pitot probe could not reach to the area over the vortex flap surface. Therefore, the flowfield around the vortex flap for this configuration could not be obtained. This figure shows that a separated region is formed inboard the flap hinge line. The recirculating region between $y/(b/2) = 0.4$ and flap hinge line ($y/(b/2) = 0.75$) shows similar flow field patterns to the leading-edge separation vortex formed on the vortex flap of $d_f = 20^\circ$ (Fig. 7(b)). Note that the separation vortex was also observed on the vortex flap surface as was discussed in Fig. 5(c).

Figure 8 shows the results of the flow field measurements of total pressure isobars for $d_f = 0^\circ$, 20° and 50° at $a = 9^\circ$. The total pressure contours for $d_f = 0^\circ$ (Fig. 8(a)) shows that the total pressure losses are observed inside the leading-edge separation vortex between $y/(b/2) = 0.6$ and 1.0. This tendency is the same for the leading-edge separation vortex formed on a 76° sharp delta wing at $a = 20.5^\circ$, $Re_c = 2 \times 10^6$ in Hummel (1978). It is noted that

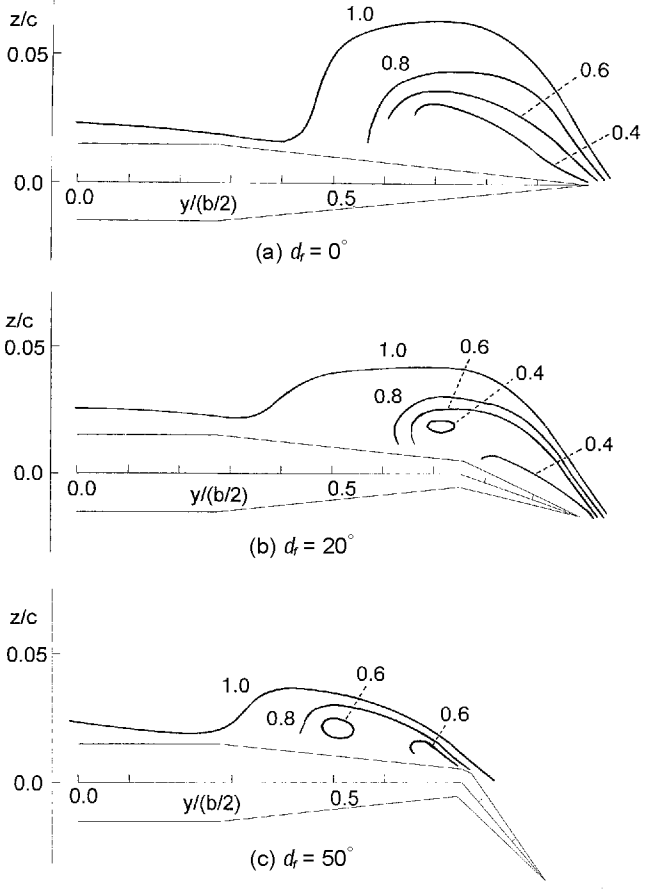

Fig. 8. Total pressure isobars at $a = 9^\circ$, $x/C = 0.55$.

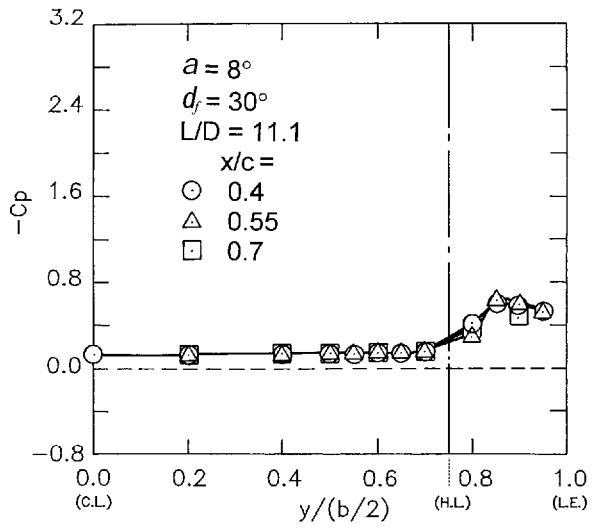

Fig. 9. Surface pressure distributions at $a = 8^{\circ}$, $d_f = 30^{\circ}$.

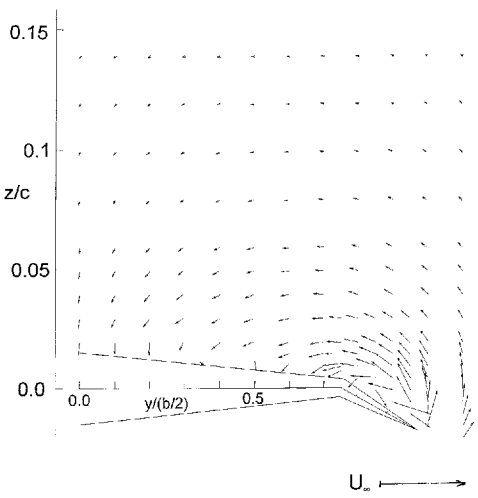

(a) $x/C = 0.4$

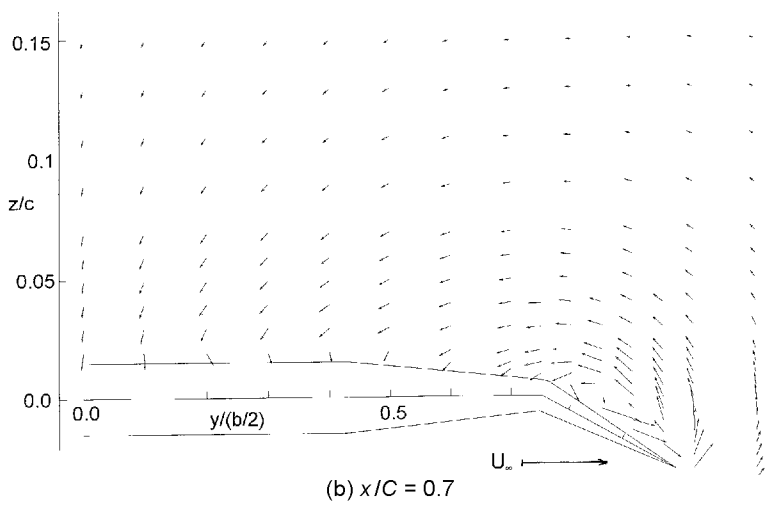

(b) $x/C = 0.7$

Fig. 10. Velocity vector components in the cross flow plane at $a = 8^{\circ}$, $d_f = 30^{\circ}$.

some data near the wing surface have not been measured as stated in Fig. 7(a). Therefore the isobars inside the leading-edge separation vortex near the wing surface should be treated with caution. The secondary separation region inside the vortex cannot be observed in this figure as discussed in Fig. 7(a).

Figure 8(b) shows the total pressure isobars for $d_f = 20^\circ$. The leading-edge separation vortex is formed on the vortex flap surface as shown in Fig. 7(b). The separation vortex formed on the vortex flap surface in Fig. 8(b) is smaller than the separation vortex on the plain delta wing at the same angle of attack in Fig.8(a). Two low-pressure isobars are observed in this Fig. 8(b), the one located inboard the flap hinge line and the other on the vortex flap surface. First one is thought to correspond to the core of the separation vortex. Second one corresponds to the secondary separation as mentioned in Fig. 7(b). Figure 8(c) shows the results for $d_f = 50^\circ$. As noted in Fig. 7(c), the flow over the flap surface was not measured. The vortex formed inboard the flap hinge line indicates the similar total pressure distributions as the one on the vortex flap surface in Fig. 8(b).

Figure 9 shows the surface pressure distributions for the upper surface at $a = 8^\circ$, $d_f = 30^\circ$ for different chordwise stations $x/C = 0.4$, 0.55 and 0.7. Near maximum lift drag ratio of 11.1 was attained at this configuration (see Fig. 3). This figure shows that almost the same pressure distributions are attained for different chordwise stations, which means that a similar flow exists along the chordwise station over the delta wing at this configuration.

Figure 10 shows the velocity vector components in the measuring plane at the same configuration as in Fig. 9 for $x/C = 0.4$ and 0.7. These figures show that the leading-edge separation vortex is formed over the vortex flap. The flow patterns of this separation vortex are the same for different chordwise stations that confirm the results observed in Fig. 9.

4. Discussion

Experimental results have shown that the magnitude and the location of the separation vortex formed on the vortex flap surface are significantly affected by the flap deflection angle. Figure 11 shows the cross flow pattern sketches for the 70° delta wings that indicate the formation and the location of the separation vortex. These flow pattern sketches were deduced mainly from the surface pressure measurements at $x/C = 0.55$, partly from the oil-flow visualization tests and partly from the 5 holes pitot probe tests at $x/C = 0.55$. This figure is plotted against the angle of attack a and the streamwise flap deflection angle d_{fs}. It is thought that the occurrence of separation on the

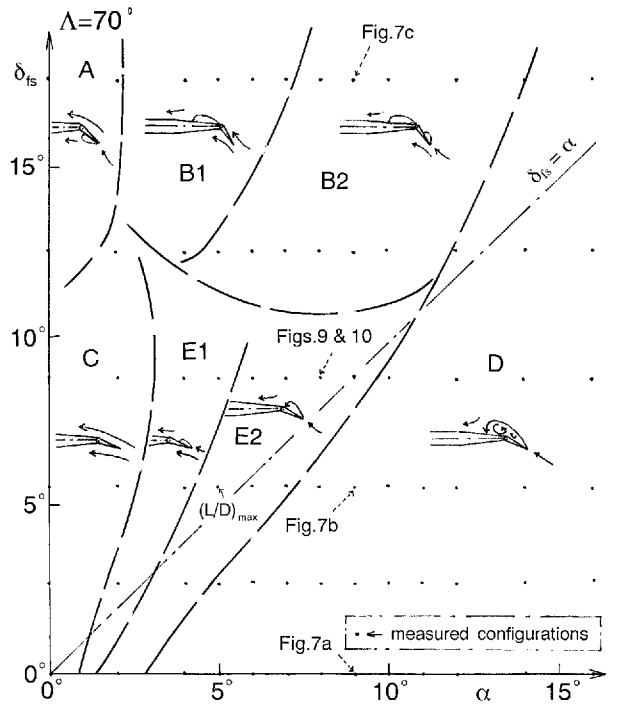

Fig. 11. Cross flow pattern sketches plotted on d_{fs} vs. a plane.

LEVF is mainly determined by the angle between the incoming flow and the flap surface. This led to the present study that accounts for a streamwise flap deflection angle d_{fs} as a parameter controlling the behavior of the lift/drag ratio. The streamwise flap deflection angle d_{fs} is derived by $d_{fs} = \tan^{-1}(\sin e \cdot \tan d_f)$, where e is a semi-apex angle of the main wing alone, i.e. inboard the flap hinge line (see Fig. 2). The wing configuration $d_{fs} = a$ means that the direction of the free stream coincides with the direction of the flap surface. When $d_{fs} < a$, the stagnation point is expected to be located on a lower surface of the flap and a separation occurs on the upper surface. When $d_{fs} > a$, it is expected that the separation would occur on the lower surface if the flow direction near the wing were parallel to the direction of the free stream. Since the flow near the wing is affected by the existence of the wing, the stagnation point may exist on the lower surface that causes the flow to separate on the upper surface, except when $d_{fs} \gg a$. It is thought that d_{fs} can be used as a parameter that is related to the occurrence of separation on the flap surface. The line $d_{fs} = a$ is plotted in Fig. 11 as a reference.

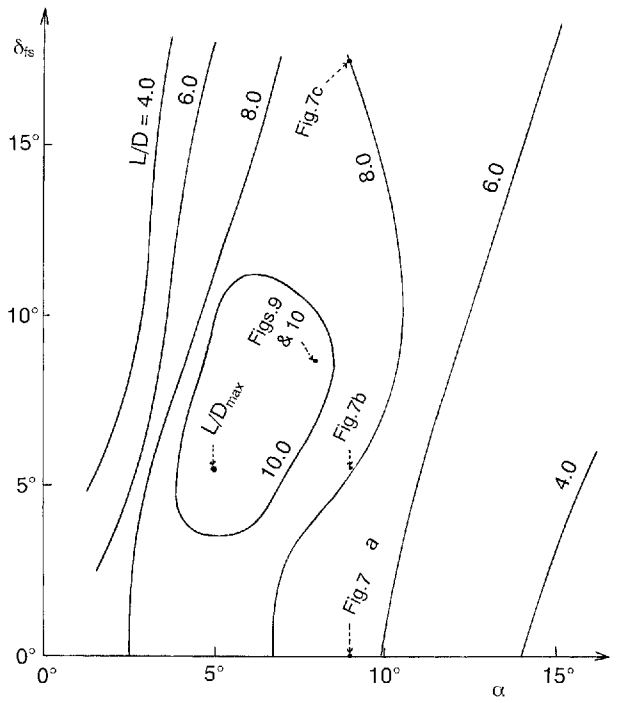

Fig. 12. *L/D* Isobars on d_{fs} vs. a.

Figure 12 is the *L/D* isobars plotted on d_{fs} vs. a. This figure shows that the improvement of *L/D* is attained at modest angles of attack (a's about 5°) and modest flap deflection angles (d_{fs}' between 5° and 10°).

Figure 11 suggests that the flow in cross flow planes around the vortex flap can be divided into several different regimes as marked A, B1, B2, C, D, E1 and E2:

(1) Regime A (at low a and high d_{fs}; $d_{fs} \gg a$): Separation occurs on lower surfaces that increases the drag acting on the wing, hence only a low *L/D* is attained (see Fig. 12).

(2) Regimes B1 and B2 (at modest a and high d_{fs}): Separation occurs inboard the flap hinge-lines (see Fig. 7(c)). In B2 area, separation also occurs on the flap surface. These separations increase the drag of the wing and decrease the *L/D*.

(3) Regime C (at low a and modest d_{fs}): Separation is not observed both on the upper and on the lower flap surface. Therefore, the drag caused by the vortex is very low, but still certain amount of the friction drag is acting on the wing. Furthermore, C_L is also very low due to the low angle of attack, hence the benefit of *L/D* cannot be observed in this area.

(4) Regime D (roughly at large a and modest d_{fs}): Since d_{fs} is lower than a, separation occurs on the upper surface that increases the drag as discussed before (see Figs. 7(a) and 7(b)). It is seen that the area where $d_{fs} < a$ roughly coincides with this regime D.

(5) Regimes E1 and E2 (at modest a and modest d_{fs}): Separation occurs on the flap surface. Reattachment point is located outboard of the flap hinge line for E1 regime. The spanwise length of the separation vortex almost coincides with the flap length in E2 regime (see Fig. 10). The maximum *L/D* is attained in this E2 regime.

Figure 12 indicates that the area where the improvement of L/D is accomplished ($L/D > 10$) almost coincides with these regimes E1 and E2. This figure also indicates that the benefit of the L/D improvements by the LEVF cannot be attained when a is much lower than d_{fs} or a is much higher than d_{fs}, as long as d_{fs} is not higher than10°, i.e. the LEVF is deflected modestly.

It is noted that the flow changes gradually among each regime. Therefore, lines plotted in Fig. 11 are not the clear borderlines. These lines should be treated with caution.

Figure 12 shows that the long axis of the maximum L/D isobars with elliptic shape is not parallel to the line of $d_{fs} = a$. This is partly caused by the fact that the flow direction near the wing is not parallel to that of the free stream as mentioned before. However, the streamwise flap deflection angle is still a good measure for the initial design phase of the vortex flap.

5. Conclusions

Measured results on a 70° delta wing with the leading-edge vortex flaps were used to investigate the behaviors of the leading-edge separation vortex formed on the vortex flaps.

(1) Separation vortices formed on a plain delta wing, on a vortex flap and inboard the vortex flap hinge line were clearly visualized.
(2) The flow around the vortex flaps is classified into several different cross flow patterns.
(3) The streamwise flap deflection angle was defined to discuss the vortex flap performance. The optimum lift/drag ratio is attained when the amount of the wing angle of attack is not far different from the amount of the streamwise flap deflection angle, as long as the vortex flap is deflected modestly.

Acknowledgments

The author would like to express his gratitude to Messrs. T. Fujita, A. Iwasaki and H. Fujieda, National Aerospace Laboratory, Japan for their help in conducting the wind tunnel experiments.

References

Campbell, J. F. and Osborn, R. F., Leading-edge Vortex Research: Some Nonplanar Concepts and Current Challenges, Vortex Flow Aerodynamics Volume I, NASA CP-2416, (1986), 31-63.

Hummel, D., On the Vortex Formation over a Slender Wing at Large Angles of Attack, High Angle of Attack Aerodynamics, AGARD CP-247, (1978), 15-1 - 15-17.

Rao, D. M., Leading-edge Vortex-flap Experiments on a 74 Deg. Delta Wing, NASA CR-159161, (1979).

Rinoie, K., Studies of Vortex Flaps for Different Sweepback Angle Delta Wings, Aeronautical Journal, 1009 (1997), 409-416.

Rinoie, K. and Stollery, J. L., Experimental Studies of Vortex Flaps and Vortex Plates, Journal of Aircraft, 31-2 (1994), 322-329.

Rinoie, K., Fujita, T., Iwasaki, A. and Fujieda, H., Experimental Studies of a 70-degree Delta Wing with Vortex Flaps, Journal of Aircraft, 34-5 (1997), 600-605.

Author Profile

Kenichi Rinoie: He received his M. eng. degree in Aeronautics in 1984 from The University of Tokyo. He recived Dr. Eng. degree in Aeronautics in 1988 from The University of Tokyo. He worked in Department of Aeronautics, The University of Tokyo as a research associate, in National Aerospace Laboratory as a senior researcher and in College of Aeronautics, Cranfield University as a visiting research fellow. He has been working in Department of Aeronautics and Astronautics, The University of Tokyo as an associate professor since 1993. His research interest covers aircraft design, separated flow aerodynamics and pilot human factors. He is a member of Royal Aeronautical Society (MRAeS, CEng).